Microwave and Optical Technology Letters

WILEY

RESEARCH ARTICLE

W-Band High-Efficiency Low-Profile Four-Folded Transmitarray Antenna Based on Dual-Phase Compensation Strategy

Xianhui He[1] | Lu Cong[1] | Yongzheng Li[1] | Quan Xue[1] | Wanchen Yang[2]

[1]Guangdong Provincial Key Laboratory of Millimeter-Wave and Terahertz, Guangdong-Hong Kong-Macao Joint Laboratory for Millimeter-Wave and Terahertz, School of Electronic and Information Engineering, South China University of Technology, Guangzhou, P. R. China | [2]College of Electronic and Information Engineering, Nanjing University of Aeronautics and Astronautics, Nanjing, P. R. China

Correspondence: Wanchen Yang (wcyang@nuaa.edu.cn)

Received: 24 October 2024 | **Revised:** 26 March 2025 | **Accepted:** 7 August 2025

Funding: This study was supported by National Natural Science Foundation of China (61931009) (62321002) (62471219).

Keywords: dual-phase compensation | folded transmitarray | low profile | millimeter wave band | single-layer PCB

ABSTRACT

A novel high-efficiency low-profile four-folded transmitarray antenna (FTA) is proposed. The FTA is composed of a dual-functional transmit-reflected array (TRA) and a polarized conversion surface (PCS) based on single-layer PCB. The work proposed a novel dual-functional transmit-reflected element and dual-phase compensation strategy. Firstly, dual-functional transmit-reflected element is composed of double pairs of U-shaped and cross-shaped patches to realize efficient transmission and reflection, with the losses under 2 dB. Thus, high-efficiency dual-functional transmit-reflected array can be achieved. Secondly, dual-phase compensation strategy for primary and secondary arrays is put forward to realize low profile folding configuration, which is capable of achieving a profile compression ratio of no more than 0.25. Different from conventional FTA designs, no polarized grids, metal vias or bonding layers are required. For demonstration, one FTA prototype working in W-band is designed, fabricated and measured. The total size of the FTA is about $60 \times 60 \times 15.75\ \text{mm}^3$. The measured peak gain and aperture efficiencies are 28.68 dBi and 21.38% at 89 GHz with 3-dB gain bandwidth of 10%, which achieved the highest gain and aperture efficiency in current W-band research. Benefiting from high-efficiency, low-profile, single-layer fabrication, as well as easy integration, the proposed FTA is expected to be a competitive candidate for vehicle radar and LEO satellites communication systems in high frequency of millimeter wave band to terahertz band.

1 | Introduction

Owing to the large bandwidth, ultrahigh data rate and ultrahigh resolution, W-band (75–110 GHz) has attracted much attention in potential B5G/6G wireless communication, such as radar detection and satellite systems [1, 2]. As the boundary frequency between millimeter wave (MMW) and terahertz wave band, the loss increases severely and wavelength reduces sharply with frequency increases [3]. Therefore, W-band antenna faces urgent problems such as dielectric loss, transmission loss and manufacturing constraints.

To overcome the severe losses, high directivity antenna is an effective antenna type to obtain desired radiation performance. Therein, reflectarray (RA) and transmitarray (TA) antennas have shown immense potential in satellite communication systems [4] and reconfigurable intelligent surface (RIS) [5], and greatly expanded multi-scenario wireless communication adaptability of the antennas. However, the profile of high-gain TA and RA are relatively high (at least 10 λ), which requires high assembly accuracy and increases the design complexity [6, 7]. To reduce the overall profile of RA/TA, folded reflect/transmit-array antenna (FRA/FTA) is proposed based on the ray tracing method, and the overall profile can be reduced to less than a half of the original height. Hence, FRA/FTA are highly suitable for communication between satellites and ground stations, particularly for low-earth-orbit (LEO) satellites, vehicle radars or user terminals, which have stringent requirements for size and weight.

In most state-of-the-art FTA studies, multiple metal and air layers (at least 3 metal layers), metal vias, polarized grids and adhesive layers are indispensable [8–11]. A planar substrate integrated waveguide (SIW) slot array is adopted as the primary source in the proposed FRA [8], which obtained a peak boresight gain of 31.9 dBi. However, the profile remains half of the original height. In [9], benefiting from the polarizer and polarization conversion arrays, the folded array profile compression ratio H/F is compressed to 0.33, however, the aperture efficiency is less than 14%. In [10], high aperture efficiency of the FTA reaches 51% and wide 3-dB gain bandwidth of more than 27% are achieved at 10 GHz. However, four metal layers and three air layers are adopted, which poses high requirements for processing and assembling. In [11], a receiver–transmitter metasurface (RTMS) composed of "3-layer-sandwich" stuctures (receiving patch, ground plane, and transmitting patch) is proposed to separate dual polarizations, and the peak aperture efficiency of two circular polarizations are about 40% at 10 GHz. However, the three metal layers and metal vias are needed. Thus, it is difficult to achieve a balance between high aperture efficiency and low profile. It can be seen, in high frequency band of MMW and terahertz, the problem of bonding films between multilayers cannot be ignored due to the increasing dielectric loss with frequency. Meanwhile, multi-layer structures are bound to cause assembly errors, further deteriorating the radiation efficiency inevitably. Therefore, there remains significant potential for enhancing the aperture efficiency and reducing the profile height of existing FTA.

In this study, a novel dual-functional transmit-reflected element and dual-phase compensation strategy are proposed to satisfy efficient FTA with low profile array structures in high frequency band of MMW. Based on the double pairs of U-shaped and cross-shaped patch structures, dual-functional transmit-reflected element can be realized, which is an effective approach to reduce the profile. According to the dual-phase compensation strategy for primary and secondary arrays, low profile compression ratio of no more than 0.25 (four-folded) can be achieved. Using standard one-layer PCB process, the FTA prototype is fabricated and measured. According to the experimental results, the proposed four-folded transmitarray achieves the highest gain and aperture efficiency in the current W-band designs, while maintaining a quarter of original array profile. Therefore, profiting from high efficiency, low profile, ultra-thin thickness, easy fabrication and low cost, the proposed four-folded FTA is a promising candidate for vehicle radar and LEO satellites communication in high frequency band of millimeter to terahertz band.

2 | Transmit-Reflected Element and Polarization Conversion Surface Element Design

To realize FTA with fewer layer structures, one effective approach is using dual-functional transmit-reflected array (TRA). Accordingly, to enhance the aperture efficiency of FTA, an efficient transmit-reflected element design is much essential. Therefore, low-loss dual-functional transmit-reflected element would be studied first. Then, polarization conversion surface (PCS) element is also designed in this section.

2.1 | Design of Dual-Functional Transmit-Reflected Element and Polarization Conversion Surface Element

The element structure of the proposed dual-functional transmit-reflected element and PCS element structures are shown in Figure 1. Both the transmission and reflection element are composed of patches located on two sides of a single layer dielectric substate. As seen in Figure 1A, there are two dual-pair of U-shaped patches on the two surfaces of the substrate, which are in the opposite orientations in Y-direction and composed of the transmission element. Similarly, there is a cross strip on the top surface and another wider strip on the bottom surface, which composed of the reflection element in X-direction. The relevant parameters are as follows, $P = 2$ mm, $h = 0.508$ mm, $d = w_0 = 0.07$ mm, $w_1 = 0.11$ mm, $L_{S10} = 1.25$ mm, $L_{S20} = 1.2$ mm. The detailed principle will be explaned later. As shown in Figure 1B, a reflected PCS element with two bending strips and metal ground is proposed. The period of PCS element is set to be $P_c = 0.34\ \lambda_0$, about 1.2 mm, and the strip length is $l = 0.6$ mm, with the width of $w = 0.1$ mm, $g = 0.035$ mm.

By constructing a balance of electric and magnetic resonance of Huygens metasurface (HMS) [12], efficient transmission can be stimulated. According to the generalized sheet transition conditions (GSTC) [13], by inducing discontinuities in tangential magnetic and electric field components, HMS can be

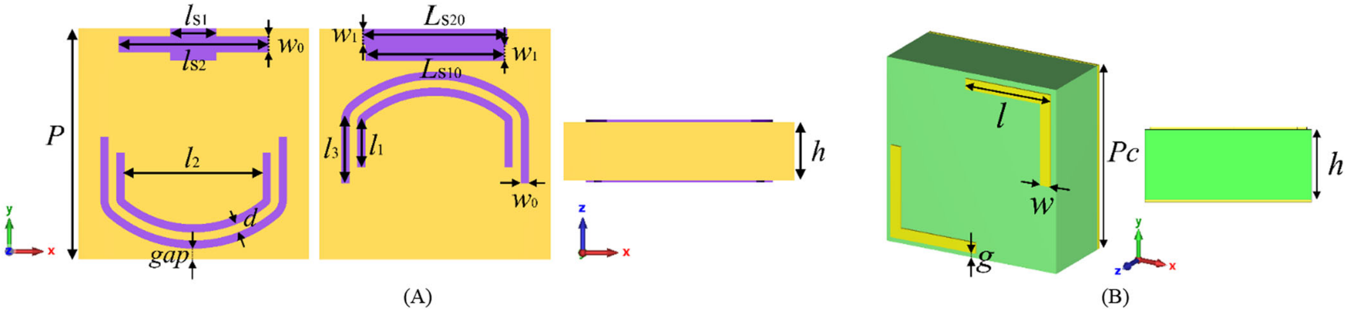

FIGURE 1 | (A) Structure of dual-functional transmit-reflected element. (B) Structure of the reflected $_{PCS}$ element.

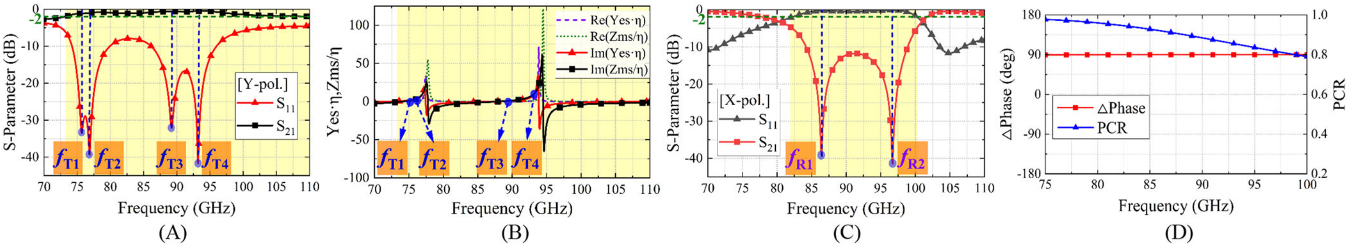

FIGURE 2 | (A) Normalized admittance and impedance of the proposed dual-functional transmit-reflected element. (B) S-parameters of Y-pol. transmission element. (C) S-parameters of X-pol. reflection element. (D) Polarization conversion rates (PCR) and phase differences (△Phase) of PCS element.

characterized by its surface impedance Z_{ms} and admittance Y_{es}, respectively. To achieve ideal near-unity transmission ($S_{11} = 0$, $S_{21} = 1$), normalized electric surface admittance should be equal to magnetic surface impedance:

$$\mathrm{Re}(\eta_0 Y_{es}) = \mathrm{Re}\left(\frac{Z_{ms}}{\eta_0}\right) = 0,\ \mathrm{Im}(\eta_0 Y_{es}) = \mathrm{Im}\left(\frac{Z_{ms}}{\eta_0}\right) \quad (1)$$

where η_0 is wave impedance of free space. For the proposed transmission element working in Y-polarization (Y-pol.), if the $\eta_0 Y_{es}$ and Z_{ms}/η_0 are equal and purely imaginary, Huygens resonance is excited. Detailed element construction methods were proposed in previous study [14]. To construct the balance of electric and magnetic resonance, normalized admittance and impedance of the proposed dual-functional transmit-reflected element is shown in Figure 2A. The imaginary parts of $\eta_0 Y_{es}$ and Z_{ms}/η_0 are equal at f_{T1} to f_{T4}, whereas their real parts are near zero. According to Equation (1), four balance frequencies of electric and magnetic resonance are achieved, thus, a large bandwidth of high-transmission is achieved from 73 GHz to 110 GHz, as shown in the yellow shaded area. The S-parameters of the proposed transmission element is shown in Figure 2B. Four poles from f_{T1} to f_{T4} are observed in S_{21}, indicating the large bandwidth of the efficient transmission. Similarly, for the X-polarization (X-pol.) reflection element, by constructing multi-resonance frequencies induced by the cross-shaped patches in X-direction, efficient reflection bandwidth can be expanded. The S-parameters are shown in Figure 2C. two reflection resonances occurred at f_{R1} and f_{R2}. Subsequently, a large reflection bandwidth with low loss below 2 dB is realized, about 82~100.3 GHz. As shown in Figure 2D, in a very wide frequency range from 75 to 100 GHz, the reflected polarization conversion rates are above 0.8, and phase differences between reflected and incident wave are maintained to be 90°, indicating the element has broadband polarization conversion performance.

2.2 | Independent Performance of Dual-Functional Transmit-Reflected Element Library

After analyzing the working principle of proposed dual-functional transmit-reflected element, the following will establish two element libraries to cover the required 360° phase range in both transmission and reflection mode. As seen in Figure 1A, by adjusting the overlapped length of l_1, l_2, l_3 and *gap*, the transmission phase can be shifted. Similarly, the reflection phase changes with the strip length l_{S1} and l_{S2}. Subsequently, the performance of transmission and reflection element libraries are constructed, as shown in Figure 3.

It can be seen in Figure 3A,D, transmission and reflection losses at center frequency of 85 GHz are under 1.2 and 0.5 dB, implying efficient transmission and reflection can be achieved. The independent regulation performance of the proposed transmit-reflected element libraries is analyzed, as shown in Figure 3B,E. Reflection frequency can be shifted by adjusting strip length l_{S1} and l_{S2}, and reflection phase changes accordingly. Meanwhile, transmission phase and amplitude can be adjusted by *gap*, l_1, and l_3. The element #1~#6 in Figure 3B means different reflection elements under different cross-shaped lengths (with l_{S1}: 0.8~1.3 mm), and element #1~#6 in Figure 3E means different transmission elements under different U-shaped lengths (with l_1:1.1~1.5 mm).

It is observed that when different reflection and transmission element lengths are adopted, the transmission and reflection phase and amplitude of original element almost remain unchanged. Therefore, profiting from orthogonal polarizations, the regulations of transmission and reflection are independent. Consequently, efficient transmission and reflection can be realized simultaneously by the proposed element libraries and regulations of two modes are independent. The influences of different oblique incidence angle on the element performance ($\theta = 0°$~$30°$) are also studied, as shown in Figure 3C,F. Taking one element as an example, the key parameters of the selected element are as follows, $l_1 = 0.4$ mm, $l_2 = 1.25$ mm, $l_3 = 0.54$ mm and $gap = -0.15$ mm. Transmission performance is shown in Figure 3C, when θ changes from 0 to 25°, the transmission loss at the center frequency is less than 3 dB. When $\theta = 30°$, the transmission loss exceeded 4 dB. The reflection performance is shown in Figure 3F, similarly, the reflection loss is less than 2 dB. When θ is greater than 25°, the transmission loss is bigger than 2 dB. In addition, the transmission and reflection phase change a little with different θ, which are almost unaffected by the incident angle. Therefore, for the dual-functional transmit-reflected element, the maximum angle for stable performance can be set to be 25°.

3 | High-Efficiency Low-Profile Four-Folded Transmitarray Antenna Based on Dual-Phase Compensation Strategy

3.1 | Configuration of Four-Folded Transmitarray Antenna

The dual-phase compensation strategy of primary and secondary arrays is proposed, as shown in Figure 4. The proposed FTA is consisted of three components, including one dual-functional TRA, one polarized conversion surface (PCS), and one feed antenna. The actual FTA structure and equivalent structure are presented in Figure 4A,B, respectively.

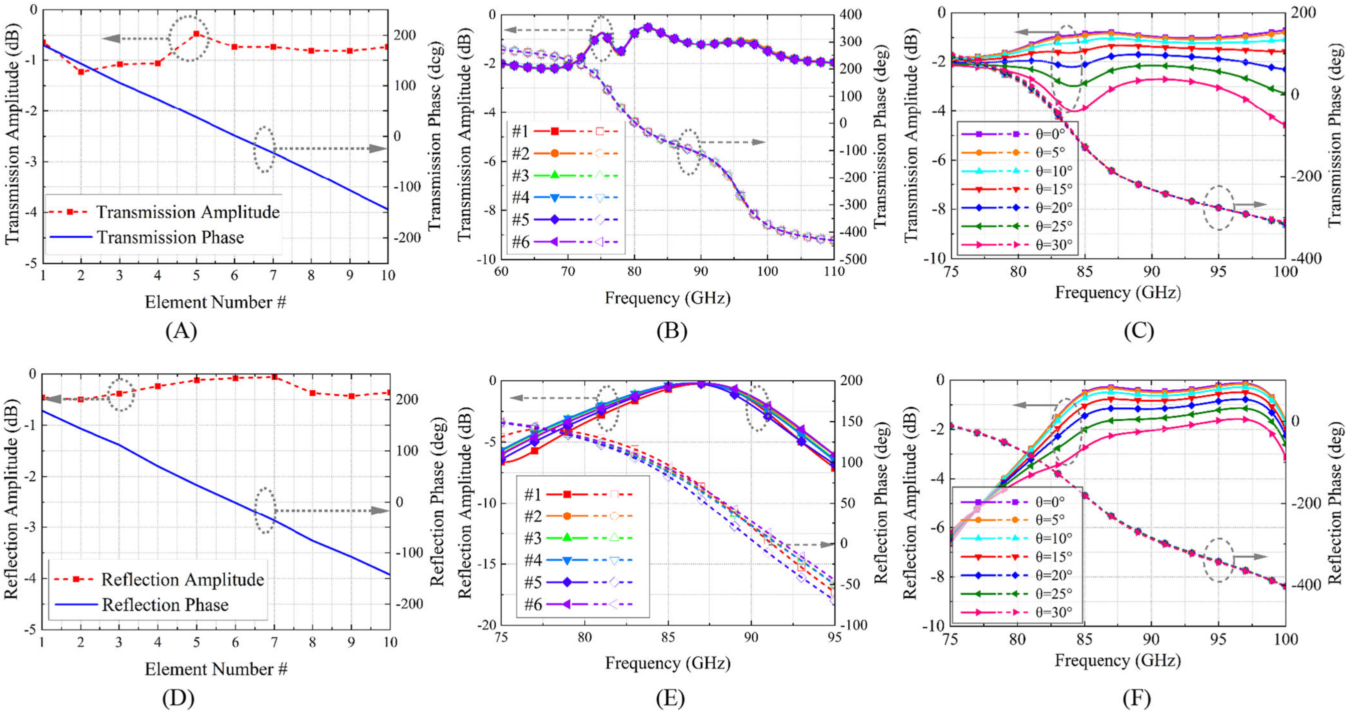

FIGURE 3 | Amplitude and phase of (A) transmission and (D) reflection element library. (B) Transmission performance under different reflection dimensions, #1~#6, with l_{S1}: 0.8~1.3 mm. (E) Reflection performance under different transmission dimensions, #1~#6, with l_1:1.1~1.5 mm. The transmit-reflected element performance ($\theta = 0°$~$30°$). (C) Transmission performance under different oblique incidence angles, (F) reflection performance under different oblique incidence angles.

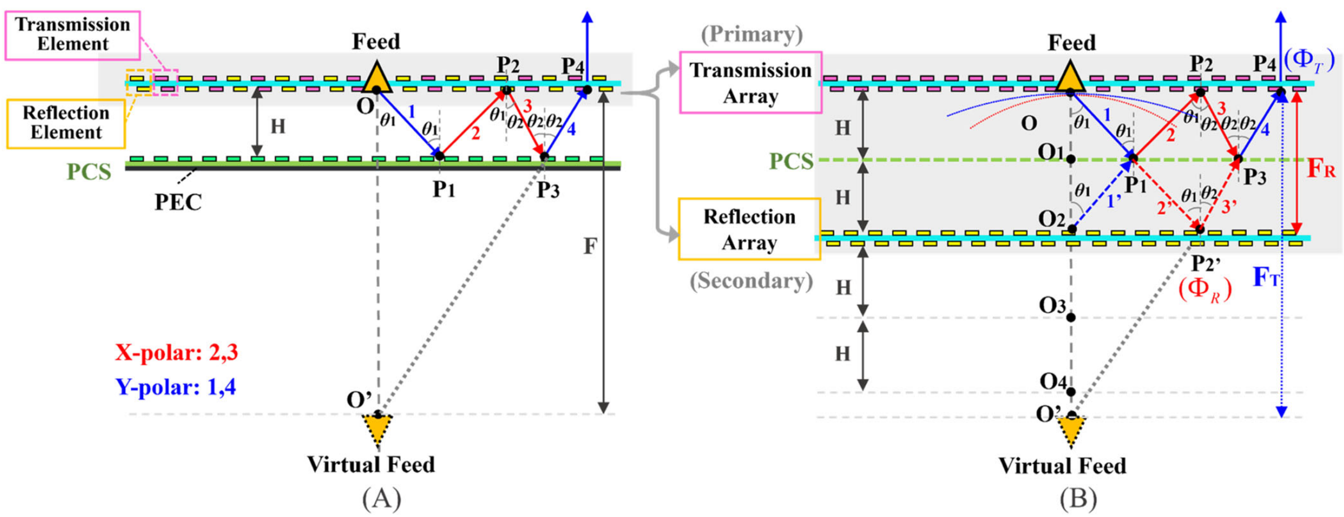

FIGURE 4 | Schematic of the four-folded FTA in side view. (A) Actual FTA structure and (B) equivalent FTA structure.

As shown in Figure 4A, the feed is simplified as a point 'O', serving as the phase center of actual feed, and operating at Y. pol. Based on the ray tracing principle, the wave paths are labeled as '1'~'4'. The Y. pol propagating wave '1' is reflected at P_1 and converted to X. pol as wave '2', due to the presence of reflective PCS. Then, phase compensation occurs at P_2 while performing co-polarized reflection, named wave '3'. Similarly, the polarization conversion reflection occurs again at P_3, Y. pol wave '4' comes to P_4 to realize phase compensation and co-polarized transmission to form focus beam at last. As seen, the total wave paths are expressed as $|OP_1| + |P_1P_2| + |P_2P_3| + |P_3P_4|$. It is worth noting that co-polarized phase compensations occurred at P_2 and P_4, in reflection and transmission modes, respectively. According to independent modulations of two orthogonal LPs, the dual-functional array can be divided into two arrays: TA and RA, primary and secondary array, namely, so the FTA structure is equivalent to Figure 4B. That's to say, the FTA design can be simplified to two independent RA and TA designs, which can be regarded on the two sides of PCS with the distance of H. Subsequently, the equvalent paths can be expressed as $|OP_1| + |P_1P_{2'}| + |P_{2'}P_3| + |P_3P_4|$. Thus, the phase compensations are occurred at $P_2{}'$ and P_4, which are denoted as Φ_R and Φ_T, respectively.

In fact, because there are three times of reflection and one time of transmission occurred during the wave propagation, a four-folded FTA architecture is formed. When the phase compensation of RA is not adopted (only serves as a reflector), there is $\theta_1 = \theta_2$, the profile of FTA (H) can be compressed to a quarter. Saying, the profile compression ratio $k = H/F = 0.25$, where F is the original profile without compression. Therefore, if RA provides certain phase modulation simultaneously, which means θ_1 is not equal to θ_2, thus, $k < 0.25$. Specifically, TA plays the role of primary array of phase modulation, while RA acts as the secondary array of phase modulation, and PCS is a unity reflection array, providing polarization rotation without phase control. Therefore, benefiting from the dual-phase compensation strategy of primary and secondary arrays, the profile compression ratio can be compressed to less than 0.25 in the proposed FTA. As mentioned earlier, the phase compensation includes reflection part at P_2' with X. pol and transmission part at P_4 with Y. pol. For the TA and RA, the focal lengths are marked as F_T and F_R. When considering the phase modulation of P_2', before the phase modulation, there is a spherical wave with radius of F_R, and after the phase modulation, there is a spherical wave with radius of F_T. Thus, the reflection phase compensation value at P_2' is obtained by converting the spherical wave with radius F_R to F_T. Therefore, the phase compensation of RA is calculated as

$$\begin{aligned}\Phi_{R,x-pol} = &\frac{2\pi}{\lambda}\Big[\sqrt{x_x^2(m,n) + y_x^2(m,n) + F_R^2} \\ &- \sin\theta_1(\cos\phi_1 x_x + \sin\phi_1 y_x)\Big] \\ &- \frac{2\pi}{\lambda}\Big[\sqrt{x_x^2(m,n) + y_x^2(m,n) + F_T^2} \\ &- \sin\theta_2(\cos\phi_2 x_x + \sin\phi_2 y_x)\Big] + \Delta\varphi\end{aligned} \tag{2}$$

where $x_x(m,n)$, $y_x(m,n)$ are the element coordinates at position (m,n) in RA, λ is the air wavelength at center frequency,$\Delta\varphi$ is the reference phase. (θ_1, ϕ_1) and (θ_2, ϕ_2) are the pointing angle of the target outgoing beam of RA and TA. As for P_4, the phase compensation calculation of TA is simpler, just need to compensate the phase of focused beam generated by TA with focal diameter of F_T, which can be calculated as:

$$\begin{aligned}\Phi_{T,y-pol} = &\frac{2\pi}{\lambda}\Big[\sqrt{x_y^2(m,n) + y_y^2(m,n) + F_T^2} - \sin\theta_2 \\ &(\cos\phi_2 x_y + \sin\phi_2 y_y)\Big] + \Delta\varphi\end{aligned} \tag{3}$$

where $x_y(m,n)$, $y_y(m,n)$ are the element coordinates at position (m,n) in TA. Moreover, according the schematic of proposed FTA, mathematical relationship of F/D (focal length to diameter ratio) between the RA and TA can be expressed as

$$ratioRA = \frac{2k \cdot ratioTA}{1 - 2k} \tag{4}$$

Therefore, the ratio of RA (*ratioRA*) is determined by profile compression ratio k and F/D of TA. In fact, there is a certain constraint relationship between the two factors. The ratio of TA (*ratioTA*) is relied on the beam bandwidth of feed source, while the compression ratio k is relevant to the maximum oblique incidence angle θ_{max} of array elements:

$$\theta_{max} = \arctan\frac{1 - 2k}{4k \cdot ratioTA} \tag{5}$$

In this design, considering the oblique performance of the proposed dual-functional array, the *ratioRA* is set to be 1.05, where $k = 0.25$ and $\theta_{max} = 25.46°$. It should be pointed out, if the dual-functional array obtains stable performance under larger θ_{max}, k could be further reduced. The hybrid HMS is composed of 30×30 elements, $ratioRA = ratioTA = 1.05$, H = 15.75 mm, H/D = 0.2625. To avoid the blocking effect of feed source, an oblique pointing angle of target beam is adopted, that is to say,$(\theta_2, \phi_2) = (25°, 0)$. The required phase distribution of Y. pol TA and X. pol RA are calculated based on Equations (2) and (3), the realized phase, loss, element index and phase errors between required are shown in Figure 5. Small actual phase errors within 17° and small realized losses under 1.2 dB are observed in Y. pol TA. Notably, due to *ratioRA* and *ratioTA* being equal, the required phases of RA remain 0°. It is understandable, when $k = 0.25$, RA only provides co-polarization efficient reflection without phase control.

3.2 | Performance of Four-Folded Transmitarray Antenna

The ultra-low profile four-folded FTA is fabricated with standard printed circuit board (PCB) technology and measured in compact antenna test range system (CATR), as shown in Figure 6. The overall assembly FTA structure is shown in Figure 6A. In the actual fabrication, margins are added around the array, and square structures were added on the array corners for drilling and assembling. Eight nylon support columns are assembled through holes. Both the TRA and PCS are made of single-layer of dielectric substrate, using Rogers RT/duroid 5880 substrate ($\varepsilon_r = 2.2$, $\tan\delta = 0.0009$). The far field radiation performance is measured in the CATR system, the measurement environment and equipments are shown in Figure 6B. For test convenience, a

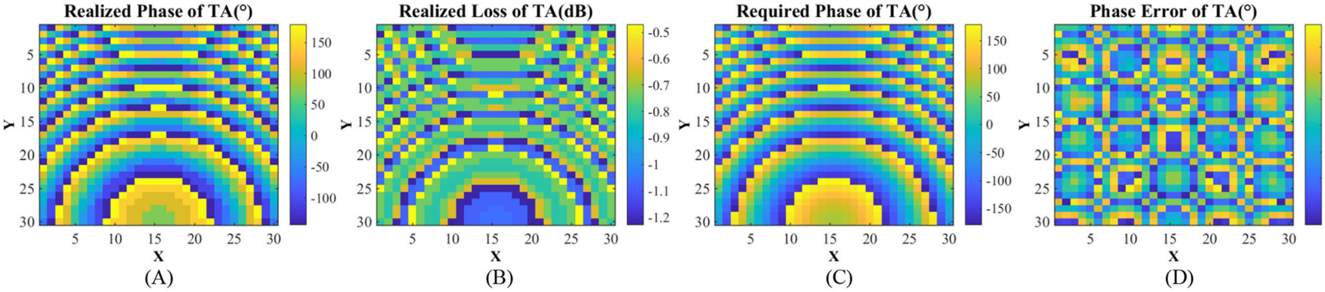

FIGURE 5 | Calculation of the Y. pol distribution. (a) Realized phase, (b) realized loss, (c) required phase and (d) phase error distributions.

3D-print support frame structure is designed to obtain the horizontal direction of transmission beam. To avoid the blocking effect of the horn flange, a 12-dBi standard gain horn with long waveguide is designed and fabricated.

The measured and simulated reflection coefficients are shown in Figure 7A. Good impedance matchings are observed within wide frequency range from 75 to 110 GHz. And simulation and actual measurement results are in good agreements. Figure 7B shows the realized gain and aperture efficiency of proposed FTA. It can be seen that the trend of measured gain and aperture efficiency curves is consistent with the simulation, indicating good consistency between the simulation and measurement. It is worth mentioning the effective area of aperture efficiency should subtract the area of the blocking parts. Thus, the realized gain of 28.23 dBi and aperture efficiency of 21.14% are realized at center frequency. Peak gain of 28.68 dBi and aperture efficiency of 28.78% are realized at 89 GHz. The yellow shadow area denoting the 3-dB gain bandwidth (BW) from 83 to 91.5 GHz (10%). The discrepancy about 1.34 dB between simulation and measurement is observed, indicating the overall loss of fabrication, mainly attributed to the waveguide loss, PCB fabrication errors, dielectric loss and assembly tolerance.

The normalized radiation patterns of proposed FTA with simulated/measured results from 83 to 90 GHz are shown in Figure 8. Good consistency can be observed between simulated and measured results. The measured main beam widths are around 5°,

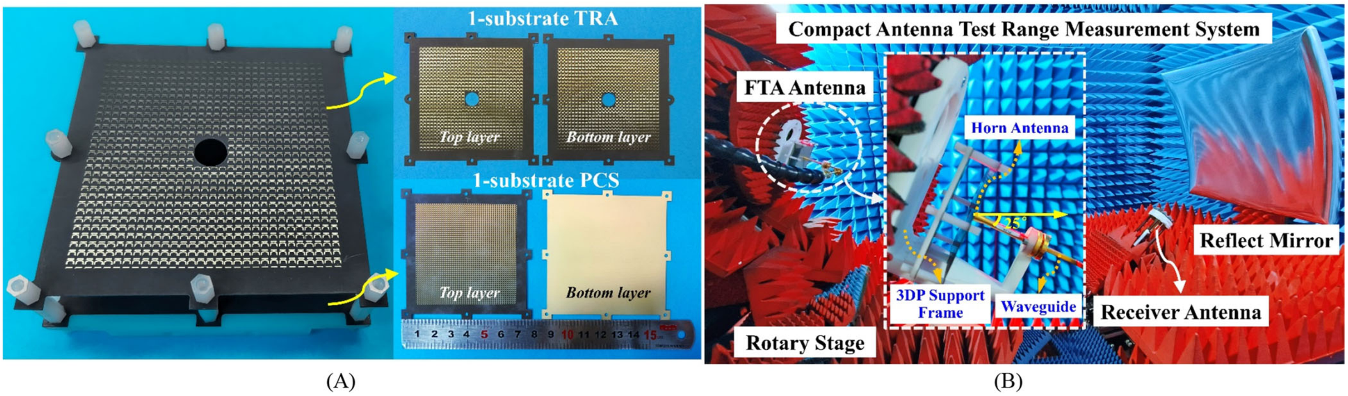

FIGURE 6 | (A) Overall assembly FTA structure. (B) Photograph of the compact antenna test range measurement system.

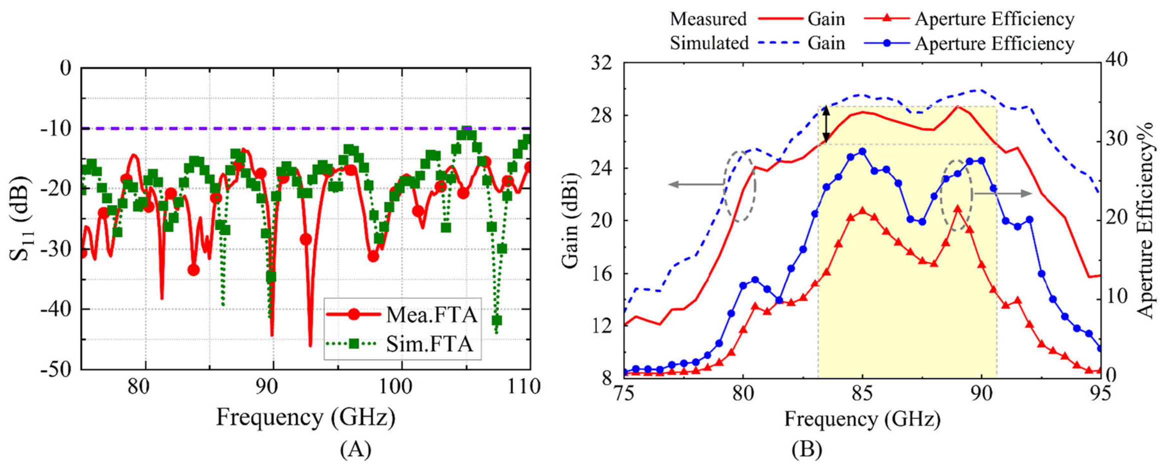

FIGURE 7 | (A) Measured (Mea.) and simulated (Sim.) S_{11} of proposed four-folded FTA. (B) Realized gain and aperture efficiency of proposed four-folded FTA.

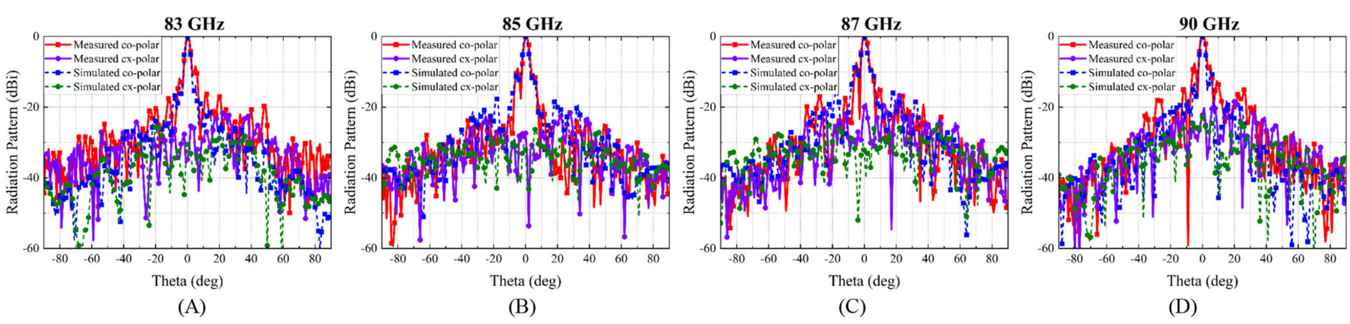

FIGURE 8 | Normalized radiation patterns (along E-plane) of the fabricated four-folded FTA. (A) 83 GHz, (B) 85 GHz, (C) 87 GHz, (D) 90 GHz.

TABLE 1 | Key performance comparisons with previously reported low-profile TA/RA.

Ref. year	Fre. (GHz)	Top layers	Bottom layers	Fabrication	Folding ratio	Strategy	H/F	H/D	Elements	Peak gain (dBi)	Peak aperture efficiency	3-dB BW
[15] 2020	12.5	1	2	2-layer PCB	2-folded	1 polarizer grid + RA	0.5	0.25	14*14	17.1	13.2%	17%
[16] 2021	10.3	3	2	2-layer PCB	3-folded	PCS + TA	0.33	0.16	17*17	21.94	21.8%	11.6%
[17] 2024	10	2	2	1-layer PCB	3-folded	RA + TA	0.33	0.18	16*16	22	X. Pol:25% Y. Pol:24.6%	9% 8.5%
[18] 2023	100	3	3	2-layer PCB	Field coupling	RA + PRS + GND	/	0.285	15*15	20.7	10.5%	15.2%
[19] 2024	148	3	2	2-layer PCB	3-folded	2 polarizer grids +TA + PCS	0.33	0.23	48*48	22	12.66%	11.7%
This study	85	2	2	1-layer PCB	4-folded	TRA + PCS	0.25	0.25	30*30	28.68	21.38%	10%

which are the same as the simulated ones. A certain degree of deterioration in the sidelobe valve are observed at 83 and 90 GHz. It is caused by the blocking of the feeding horn flange and the bent waveguide. Slight co-polar deviations between measured and simulated results existed, which are attributed to polar-direction alignment errors. However, the blocking effects of the flange and feeding waveguide are acceptable.

Table 1 compares the key performance of the proposed four-folded FTA and its counterparts. It can be seen, the proposed design has advantages of high-efficiency and big-bandwidth in the current W-band research. Compared with other low profile transmitarray antennas in similar frequency bands, the proposed FTA achieved the lowest profile, highest gain and highest aperture efficiency in the current high millimeter-wave band (75~110 GHz), while maintaing high-efficiency and low-profile simultaneously. Meanwhile, in contrast with other planar PCB FTAs [9, 15, 16], the proposed four-folded FTA design can be implemented using only single-layer PCB technology, and the top and bottom layers are only composed of 2-layer metasurfaces, which greatly simplifies the design process in conventional FTA. Most importantly, different from conventional FTAs, no polarized grids, metal vias metal grounds, or bonding layers are required. Thus, the proposed design avoids the losses caused by multi-layer bonding and greatly reduces the assembly errors in the measurement.

4 | Conclusion

In this letter, a novel high-efficiency low-profile four-folded FTA is proposed, which is composed of a dual-functional TRA and a PCS based on single-layer PCB. A novel efficient and independent dual-functional transmit-reflected element and dual-phase compensation strategy for primary and secondary arrays are put forward. An ultra-low profile four-folded FTA working in W-band is designed, fabricated and measured for demonstration. The measured results indicating the proposed FTA achieved the highest gain and aperture efficiency in the current W-band designs. Therefore, benefiting from high-efficiency, low-profile, single-layer PCB fabrication, as well as easy integration, the proposed FTA is expected to be a competitive candidate for vehicle radar and LEO satellites communication systems in high frequency band of millimeter to terahertz wave band.

Acknowledgments

This study was supported by the Science Fund for Creative Research Groups of the National Natural Science Foundation of China under Grant 62321002, in part by the National Natural Science Foundation of China under Grant 61931009 and 62471219.

Data Availability Statement

The authors have nothing to report.

References

1. S. Zheng, X. Xia, R. Lu, et al., "A 94-GHz 16T1R Hybrid Integrated Phased Array With ±50° Scanning Range for High-Date-Rate Communication," *IEEE Transactions on Circuits and Systems I: Regular Papers* 71, no. 2 (February 2024): 948–961, https://doi.org/10.1109/TCSI.2023.3335324.

2. S. Tiwari, M. Kumari, V. Kikan, R. Gill, A. Kumar, and M. Sharma, “A Novel Design Evolution of mmWave W-D Bands Modified Rectangular Patch Antenna With Circular and Rectangular Slots for Future IoT Applications,” *2023 6th International Conference on Contemporary Computing and Informatics (IC3I)*, Gautam Buddha Nagar, India, 2023, pp. 1843–1848, https://doi.org/10.1109/IC3I59117.2023.10397852.

3. F. Foglia Manzillo, A. Clemente, and J. L. Gonzalez-Jimenez, “High-Gain D -Band Transmitarrays in Standard PCB Technology for Beyond-5G Communications,” *IEEE Transactions on Antennas and Propagation* 68, no. 1 (January 2020): 587–592, https://doi.org/10.1109/TAP.2019.2938630.

4. B. Ma, F. Lu, G. Zhi, et al., “Development of an X-Band Reflectarray Antenna for Satellite Communications,” *Scientific Reports* 11, no. 1 (March 2021): 6530, https://doi.org/10.1038/s41598-021-85132-6.

5. Z. Zhang, L. Dai, X. Chen, et al., “Active RIS vs. Passive RIS: Which Will Prevail in 6G?,” *IEEE Transactions on Communications* 71, no. 3 (March 2023): 1707–1725, https://doi.org/10.1109/TCOMM.2022.3231893.

6. R. Deng, F. Yang, S. Xu, and M. Li, “A 100-GHz Metal-Only Reflectarray for High-Gain Antenna Applications,” *IEEE Antennas and Wireless Propagation Letters* 15 (2016): 178–181, https://doi.org/10.1109/LAWP.2015.2436824.

7. Q.-Y. Guo and H. Wong, “155 GHz Dual-Polarized Fabry–Perot Cavity Antenna Using Ltcc-Based Feeding Source and Phase-Shifting Surface,” *IEEE Transactions on Antennas and Propagation* 69, no. 4 (April 2021): 2347–2352, https://doi.org/10.1109/TAP.2020.3019528.

8. M. Jiang, W. Hong, Y. Zhang, S. Yu, and H. Zhou, “A Folded Reflectarray Antenna With a Planar SIW Slot Array Antenna as the Primary Source,” *IEEE Transactions on Antennas and Propagation* 62, no. 7 (July 2014): 3575–3583, https://doi.org/10.1109/TAP.2014.2317485.

9. Y. Ge, C. Lin, and Y. Liu, “Broadband Folded Transmitarray Antenna Based on an Ultrathin Transmission Polarizer,” *IEEE Transactions on Antennas and Propagation* 66, no. 11 (November 2018): 5974–5981, https://doi.org/10.1109/TAP.2018.2863121.

10. X. Zhong, H.-X. Xu, L. Chen, et al., “Metasurface-Assisted Broadband Circularly Polarized Folded Reflectarray Antenna,” *IEEE Transactions on Antennas and Propagation* 70, no. 11 (November 2022): 10465–10474, https://doi.org/10.1109/TAP.2022.3191432.

11. T.-J. Li, G.-M. Wang, T. Cai, H.-P. Li, J.-G. Liang, and J. Lou, “Broadband Folded Transmitarray Antenna With Ultralow-Profile Based on Metasurfaces,” *IEEE Transactions on Antennas and Propagation* 69, no. 10 (October 2021): 7017–7022, https://doi.org/10.1109/TAP.2021.3070679.

12. S. B. Glybovski, S. A. Tretyakov, P. A. Belov, Y. S. Kivshar, and C. R. Simovski, “Metasurfaces: From Microwaves to Visible,” *Physics Reports* 634 (2016): 1–72, https://doi.org/10.1016/j.physrep.2016.04.004.

13. C. L. Holloway, M. A. Mohamed, E. F. Kuester, and A. Dienstfrey, “Reflection and Transmission Properties of a Metafilm: With an Application to a Controllable Surface Composed of Resonant Particles,” *IEEE Transactions on Electromagnetic Compatibility* 47, no. 4 (November 2005): 853–865, https://doi.org/10.1109/TEMC.2005.853719.

14. X. He, W. Yang, Y. Li, Q. Xue, and W. Che, “W-Band Wideband Transmit-Array Antenna Based on Multiresonance Multimode Huygens Metasurface,” *IEEE Transactions on Antennas and Propagation* 72, no. 9 (September 2024): 7299–7304, https://doi.org/10.1109/TAP.2024.3418196.

15. Z. Wang, Y. Ge, J. Pu, et al., “1 Bit Electronically Reconfigurable Folded Reflectarray Antenna Based on p-i-n Diodes for Wide-Angle Beam-Scanning Applications,” *IEEE Transactions on Antennas and Propagation* 68, no. 9 (2020): 6806–6810, https://doi.org/10.1109/TAP.2020.2975265.

16. J. Yang, S. T. Chen, M. Chen, et al., “Folded Transmitarray Antenna With Circular Polarization Based on Metasurface,” *IEEE Transactions on Antennas and Propagation* 69, no. 2 (2021): 806–814, https://doi.org/10.1109/TAP.2020.3016170.

17. M. Wang, K. Sun, G.-B. Wu, and C. H. Chan, “On Folded Transmitarray With Dual Polarization,” *IEEE Transactions on Antennas and Propagation* 72, no. 2 (February 2024): 1343–1351, https://doi.org/10.1109/TAP.2023.3347872.

18. H. Jiang, J. Zhang, F. Yang, et al., “W-Band Low-Profile Transmit Array Based on Wideband Partially Reflecting Surface,” *IEEE Transactions on Antennas and Propagation* 71, no. 1 (January 2023): 1087–1092, https://doi.org/10.1109/TAP.2022.3184554.

19. J. L. González-Jiménez, F. Foglia Manzillo, A. Hamani, et al., “A D-Band Transmitter Achieving 57.6-Gb/s and 30-dBm EIRP Based on Channel-Aggregation 45-Nm ICs and a Low-Profile Flat Lens Antenna,” *IEEE Transactions on Microwave Theory and Techniques* 72, no. 1 (January 2024): 836–850, https://doi.org/10.1109/TMTT.2023.3323041.